Terahertz-Frequency Spin Hall Auto-oscillator Based on a Canted Antiferromagnet

O. R. Sulymenko, O. V. Prokopenko, V. S. Tiberkevich, A. N. Slavin, B. A. Ivanov, and R. S. Khymyn

Phys. Rev. Applied **8**, 064007 — Published 7 December 2017

DOI: 10.1103/PhysRevApplied.8.064007

THz-Frequency Spin-Hall Auto-Oscillator Based on a Canted Antiferromagnet

O. R. Sulymenko,[1] O. V. Prokopenko,[1] V. S. Tiberkevich,[2] A. N. Slavin,[2] B. A. Ivanov,[1,3,4] and R. S. Khymyn[5]

[1] *Faculty of Radio Physics, Electronics and Computer Systems, Taras Shevchenko National University of Kyiv, Kyiv, 01601, Ukraine*
[2] *Department of Physics, Oakland University, Rochester, MI 48309, USA*
[3] *Institute of Magnetism, National Academy of Science of Ukraine, Kyiv, 03142, Ukraine*
[4] *Naional University of Science and Technology MISiS, Moscow, 119049, Russian Federation*
[5] *Department of Physics, University of Gothenburg, 41296 Gothenburg, Sweden*

We propose a design of a THz-frequency signal generator based on a layered structure consisting of a current-driven platinum (Pt) layer and a layer of an antiferromagnet (AFM) with easy-plane anisotropy, where the magnetization vectors of the AFM sublattices are canted inside the easy plane by the Dzyaloshinskii-Moriya interaction (DMI). The DC electric current flowing in the Pt layer creates, due to the spin-Hall effect, a perpendicular spin current that, being injected in the AFM layer, tilts the DMI-canted AFM sublattices out of the easy plane, thus exposing them to the action of a strong internal exchange magnetic field of the AFM. The sublattice magnetizations, along with the small net magnetization vector $\mathbf{m}_{\mathrm{DMI}}$ of the canted AFM, start to rotate about the hard anisotropy axis of the AFM with the THz frequency proportional to the injected spin current and the AFM exchange field. The rotation of the small net magnetization $\mathbf{m}_{\mathrm{DMI}}$ results in the THz-frequency dipolar radiation that can be directly received by an adjacent (e.g. dielectric) resonator. We demonstrate theoretically that the radiation frequencies in the range $f = 0.05 - 2$ THz are possible at the experimentally reachable magnitudes of the driving current density, and evaluate the power of the signal radiated into different types of resonators, showing that this power increases with the increase of frequency f, and that it could exceed 1 μW at $f \sim 0.5$ THz for a typical dielectric resonator of the electric permittivity $\varepsilon \sim 10$ and quality factor $Q \sim 750$.

I. INTRODUCTION

One of the fundamental technical problems of the modern microwave/terahertz technology is the development of compact and reliable generators and receivers of coherent electromagnetic signals in the 0.1–10 THz frequency range [1–3]. The THz frequency range has a great potential for applications in medical imaging, security, material characterization, communications, control of technological processes, etc. There are several approaches to THz-frequency generation, including the use of free electron lasers [4, 5], quantum cascade lasers [6, 7], superconductor Josephson junctions [8], backward wave oscillators [5, 9], electro-optic rectification of laser radiation [10], etc. However, all the above mentioned sources of THz-frequency signals require rather complex setups, low temperatures, or/and can not be made sufficiently small, which greatly limits their usability in many important practical applications.

Thus, there is a temptation to use novel spin-dependent technologies to generate high-frequency electromagnetic signals. Indeed, the spintronic technology based on the dynamics of spin-polarized electric currents in thin multilayered ferromagnetic structures resulted in the development of spin-torque nano-oscillators (STNO), which are manufactured using e-beam lithography and could be tuned by the variation of both the bias magnetic field or the bias direct current [11–17]. Unfortunately, the frequencies of the signals generated by STNOs are not very high, and, typically, are limited to the interval of 1–50 GHz by the maximum bias magnetic field that can realistically be achieved in a portable spintronic device that uses ferromagnetic (FM) materials [18].

It was suggested some time ago [19–21] that one of the possible ways to substantially increase the frequency of the signals generated in magnetic layered structures is to use in them layers of AFM , that possess a very strong internal magnetic field of the exchange origin which keeps the magnetization vectors of the AFM sublattices antiparallel to each other. Although this idea has been known for quite a while, the realistic theoretical proposal for the development of THz-frequency AFM-based spintronic nano-oscillators has been published only recently [21, 22], soon after the first experimental observation of the switching of AFM sublattices under the action of a DC spin current [23, 24].

In this work we propose and theoretically analyze a THz-frequency signal generator based on a concept of a ferromagnetic spin-Hall oscillator (SHO) [11, 15, 25, 26], but where SHO free layer is made of a canted AFM (e.g. Hematite α-Fe_2O_3) that has a small net magnetization $\mathbf{m}_{\mathrm{DMI}}$ caused by the Dzyaloshinskii-Moriya interaction (DMI). We calculated the electromagnetic power emitted from the antiferromagnetic SHO due to the dipolar radiation from the rotating magnetization $\mathbf{m}_{\mathrm{DMI}}$ into the free space and into several types of transmission lines and resonators. Our analysis demonstrates that the output power P_{AC} of the AFM-based SHO increases with the generation frequency f, and could exceed $P_{\mathrm{AC}} = 1\,\mu$W at $f \sim 0.5$ THz if a high-quality dielectric resonator is used to receive the generated signal.

II. MAGNETIZATION DYNAMICS INDUCED IN AFM BY AN EXTERNAL SPIN CURRENT

It was shown previously [19–21], that when a layer of an AFM is subjected to an external spin current, e.g. coming from an adjacent current-driven layer of a normal metal (NM) with strong spin-orbital interaction and polarized along a unit vector $\mathbf{p}$, a corresponding spin-transfer torque (STT) [27, 28] is exerted on the sublattice magnetizations of the AFM. This STT can slightly tilt the AFM sublattice magnetizations $\mathbf{M}_1$ and $\mathbf{M}_2$, thus exposing them to the action of a large internal AFM magnetic field of the exchange origin, which starts to rotate the sublattice magnetizations about the vector $\mathbf{p}$ with a high angular frequency. For the experimentally achievable magnitudes of the spin current the frequencies of this current-induced rotation lie the THz range. There is, however, a fundamental problem of how to extract the AC signal corresponding of that THz-frequency rotation from the spin-current-driven AFM, as this extraction is necessary to create a functioning source of a THz-frequency — AFM-based SHO.

This AC signal can be, in principle, picked up using the spin pumping produced by the rotating AFM magnetizations and inverse spin-Hall effect (ISHE) in the adjacent NM layer. The ISHE voltage, however, is proportional to the instantaneous angular velocity of the AFM sublattices rotation, and if the anisotropy of the chosen AFM material is *uniaxial* (i.e. isotropic in the magnetization rotation plane), the AFM rotation is, obviously, uniform in time, and the ISHE voltage is constant, and does not contain any high frequency AC components.

To extract a high-frequency AC signal from a current-driven AFM material containing rotating magnetic sublattices two different approaches were suggested. In the framework of a first approach the feedbackinduced nonlinear damping was used [21] for this purpose. However, there are serious practical problems with the use of the first approach, as it strongly relies on the quality of the NM/AFM interface, and, also, requires rather high values of the spin-Hall angle in the NM. In the framework of the second approach it was suggested to use a bi-anisotropic AFM, like NiO. that has a relatively strong easy-plane anisotropy and a relatively weak easy-axis anisotropy in the perpendicular direction [22]. This additional anisotropy in the perpendicular direction creates an angular profile of the potential energy for the magnetic sublattices. An angular motion of the sublattice magnetizations $\mathbf{M_1}$ and $\mathbf{M_2}$ under the action of STT in this case is analogous to a viscous motion of a particle in a "washboard" potential under the action of a constant external force: the rotation of the magnetization vectors accelerates while moving towards the in-plane energy minima, and decelerates while moving away from them. As a result, the rotational motion of the magnetizations is not uniform in time anymore, and, therefore, can produce a high-frequency component in the voltage signal received in the NM layer through the ISHE. The ISHE voltage, which can be obtained by this mechanism, is proportional to the anisotropy in the perpendicular plane of the sublattice rotation [22] and, therefore, one needs a sufficiently high value of the anisotropy constant to produce a measurable resultant AC power. At the same time, the potential profile caused by the perpendicular anisotropy creates a barrier, which has to be overcome by the STT to start the sublattice rotation. That means that there will be a substantial threshold driving current, proportional the in-plane anisotropy constant, needed to start the generation of the AC signal. In addition, it turned out, that the AC signal created by the ISHE in a NM strongly decreases with the increase of the generation frequency, and reaches a substantial power ($> 1\mu$W) only in the range of relatively low frequencies, near the frequency of the in-plane antiferromagnetic resonance ($\sim 100 - 300$ GHz for NiO SHO [22]).

Thus, it is necessary to find a way to extract AC signals from a current-driven AFM material that does not have a considerable perpendicular anisotropy and is practically uniaxial. One of the possible AFM materials of this kind is Hematite (α-Fe_2O_3) in which the perpendicular anisotropy field $H_e \simeq 0.2$ Oe , compared to $H_e \simeq 600$ Oe in the strongly bi-anisotropic NiO.

III. AFM CANTED BY THE DZYALOSHINSKII-MORIYA INTERACTION (DMI)

In our current work, we propose a qualitatively different approach to extract the generated AC signal from the AFM layer. We propose to use in the layered structure of the SHO [22] a *canted* AFM (e.g. Hematite), where magnetic sublattices are canted inside the easy plane by the DMI. This DMI-induced canting results in the formation on a small intrinsic net magnetization vector $\mathbf{m}_{\rm DMI}$ of the AFM. It can be shown, that even the uniform rotation of the net magnetization vector $\mathbf{m}_{\rm DMI}$ with angular frequency $\omega = 2\pi f$ ($f = 0.05 - 2$ THz) leads to a substantial dipolar radiation of a high-frequency signal, that can be received by different types of *external resonators*.

Therefore, we consider below a bi-layered AFM-based SHO structure (see Fig. 1) consisting of a Pt layer and a Hematite layer placed in an external resonator. For a quantitative estimation of parameters of the proposed AFM-based SHO we used the following typical parameters of the layered structure: it was a circular disk of the radius $r_{\rm SHO} = 10$ μm and thickness $d_{\rm AFM}$ of 5 nm made of Hematite and covered by a 20 nm thick Platinum layer (see Fig. 1).

The bulk DMI inside the AFM layer leads to the canting of the magnetizations $\mathbf{M}_1$ and $\mathbf{M}_2$ of the AFM sublattices, thus creating a small net magnetization $\mathbf{m}_{\rm DMI} = \mathbf{M}_1 + \mathbf{M}_2$. The spin dynamics of an AFM with bi-axial anisotropy under the influence of a STT created by an external spin current is described by two coupled Landau-

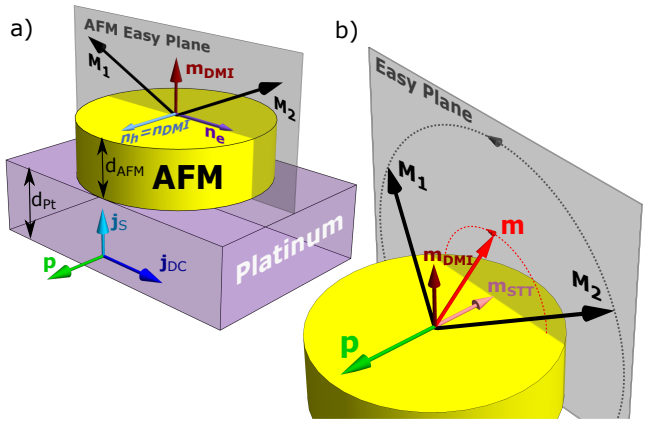

FIG. 1. a) Schematics of an auto-oscillator based on a layered structure containing a Pt layer of the thickness $d_{\rm Pt}$ and an AFM layer of the thickness $d_{\rm AFM}$. The AFM is shown in a ground state, where the sublattice magnetizations $\mathbf{M}_1$ and $\mathbf{M}_2$ lay in the easy plane of the AFM ($\mathbf{M}_1$, $\mathbf{M}_2$ $\perp$ $\mathbf{n}_{\rm h}$) and are canted by the DMI, thus producing a small net magnetization $\mathbf{m}_{\rm DMI}$. The direction of the STT polarization $\mathbf{p}$, required for the oscillations, is perpendicular to the easy plane ($\mathbf{p} \parallel \mathbf{n}_{\rm h}$), which, in turn, defines the direction of the DC: $\mathbf{j}_{\rm DC} \perp \mathbf{n}_{\rm h}$. b) The STT with polarization $\mathbf{p}$ creates magnetic moment $\mathbf{m}_{\rm STT} \parallel \mathbf{p}$. The sublattices $\mathbf{M}_1$ and $\mathbf{M}_2$, as well as the net magnetic moment $\mathbf{m} = \mathbf{m}_{\rm STT} + \mathbf{m}_{\rm DMI}$, start to rotate on a cone with a base in the AFM easy plane. The rotation trajectories are shown by dotted arcs.

Lifshitz equations for the vectors $\mathbf{M}_1$ and $\mathbf{M}_2$:

$$\frac{d\mathbf{M}_i}{dt} = \gamma\mu_0 \left[\mathbf{H}_i \times \mathbf{M}_i\right] + \\ + \frac{\alpha_{\rm eff}}{M_{\rm s}}\left[\mathbf{M}_i \times \frac{d\mathbf{M}_i}{dt}\right] + \frac{\tau}{M_{\rm s}}\left[\mathbf{M}_i \times \left[\mathbf{M}_i \times \mathbf{p}\right]\right], \quad (1)$$

where $i = 1, 2$ are the indices denoting the AFM sublattices, γ is the modulus of the gyromagnetic ratio, μ_0 is the vacuum permeability, $M_{\rm s}$ is the magnitude of saturation magnetization of the AFM sublattices, $\alpha_{\rm eff}$ is the effective AFM Gilbert damping parameter, τ is the amplitude of the STT caused by the spin current transferred from the current-driven Pt layer into the AFM layer, $\mathbf{p}$ is a unit vector along the spin current polarization, and $\mathbf{H}_i$ is the effective magnetic field acting on the sublattice $\mathbf{M}_i$:

$$\mathbf{H}_{1,2} = (-H_{\rm ex}\mathbf{M}_{2,1} - H_{\rm h}\mathbf{n}_{\rm h}\left(\mathbf{n}_{\rm h}\cdot\mathbf{M}_{1,2}\right) + \\ + H_{\rm e}\mathbf{n}_{\rm e}\left(\mathbf{n}_{\rm e}\cdot\mathbf{M}_{1,2}\right) \mp H_{\rm DMI}\left[\mathbf{n}_{\rm DMI}\times\mathbf{M}_{2,1}\right])/M_{\rm s}. \quad (2)$$

Here $H_{\rm ex}$ is the exchange field, $H_{\rm e}$ and $H_{\rm h}$ are the in-plane and perpendicular-to-plane anisotropy fields, respectively, $\mathbf{n}_{\rm e}$ and $\mathbf{n}_{\rm h}$ are the unit vectors along the "easy" and "hard" anisotropy axes, $H_{\rm DMI}$ is the effective field caused by the DMI, and $\mathbf{n}_{\rm DMI}$ is the DMI vector.

The STT amplitude expressed in the frequency units [22, 29] is:

$$\tau = j_{\rm DC} g_{\uparrow\downarrow}\theta_{\rm SH}\frac{e\gamma\lambda_{\rm Pt}\rho_{\rm Pt}}{2\pi M_{\rm s} d_{\rm AFM}}\tanh\frac{d_{\rm Pt}}{2\lambda_{\rm Pt}} \quad (3)$$

where $j_{\rm DC}$ is the density of the DC electric current in the Platinum layer, $g_{\uparrow\downarrow}$ is the spin-mixing conductance at the Pt/AFM interface, $\theta_{\rm SH}$ is spin-Hall angle in Pt, e is the modulus of the electron charge, $\lambda_{\rm Pt}$ is the spin-diffusion length in the Pt layer, $\rho_{\rm Pt}$ is the electric resistivity of Pt, $d_{\rm AFM}$ and $d_{\rm Pt}$ are the thicknesses of the AFM and Pt layers, respectively.

The effective damping parameter $\alpha_{\rm eff}$ of the layered structure in Eq.(1) includes the additional magnetic losses due to the spin pumping from the AFM layer into the adjacent Pt layer:

$$\alpha_{\rm eff} = \alpha_0 + \alpha_{\rm SP} = \alpha_0 + g_{\uparrow\downarrow}\frac{\gamma\hbar}{4\pi M_{\rm s} d_{\rm AFM}}, \quad (4)$$

where α_0 is intrinsic Gilbert damping constant, $\hbar$ is the reduced Planck constant.

As it was shown in [22], the presence of the anisotropy $H_{\rm e}$ in the plane perpendicular to the spin-polarization direction $\mathbf{p}$ makes the current-driven magnetization dynamics in AFM nonuniform in time, and, also determines the threshold charge current at which the auto-oscillatory dynamics starts. Thus, to minimize the threshold of auto-oscillations one should choose almost purely "easy-plane" AFM with $\mathbf{n}_{\rm h} \parallel \mathbf{p}$ and low value of the perpendicular anisotropy ($H_{\rm e} \ll H_{\rm h}$). The DMI vector $\mathbf{n}_{\rm DMI}$ is, commonly, directed along one of the AFM crystallographic axes. If $\mathbf{n}_{\rm DMI} \parallel \mathbf{n}_{\rm h}$, the DMI creates a small net magnetization, which lies in the easy plane of the AFM, $\mathbf{m}_{\rm DMI} \perp \mathbf{n}_{\rm h}$. The above described geometrical relations are realized, for example, in α-Fe_2O_3 (Hematite) and in $FeBO_3$.

Below, we consider in detail the SHO based on a thin film of Hematite, which has almost purely easy-plane anisotropy ($H_{\rm e} = 0.2$ Oe $= 15.9$ A/m while $H_{\rm h} = 200$ Oe $= 15.9 \cdot 10^3$ A/m, $H_{\rm ex} = 9 \cdot 10^6$ Oe $= 0.7 \cdot 10^9$ A/m) and net magnetization moment $m_{\rm DMI} = M_{\rm s} H_{\rm DMI}/H_{\rm ex} = 2100$ A/m caused by the $H_{\rm DMI} = 22 \cdot 10^3$ Oe $= 1.75 \cdot 10^6$ A/m [30–33]. The intrinsic magnetic damping of Hematite is rather low $\alpha_0 \simeq 10^{-4}$, while the effective damping that takes into account the spin pumping into the adjacent Pt layer (see Eq. (4)) is $\alpha_{\rm eff} = 2 \cdot 10^{-3}$.

We solved Eq. (1) numerically for the case when the spin current polarization $\mathbf{p} \parallel \mathbf{n}_{\rm h}$ with the main material and geometric parameters taken from [22]. In this case, the STT (i.e. the last term in Eq. (1)) tilts the AFM sublattice magnetizations $\mathbf{M}_1$ and $\mathbf{M}_2$ out of the easy plane of the AFM, and creates the net magnetic moment

$$m_{\rm STT} = \frac{\tau M_{\rm s}}{\alpha_{\rm eff}\gamma H_{\rm ex}} \quad (5)$$

in the out-of-plane direction $\mathbf{m}_{\rm STT} \parallel \mathbf{p} \parallel \mathbf{n}_{\rm h}$. Now, the total net magnetization reads as $\mathbf{m} = \mathbf{m}_{\rm DMI} + \mathbf{m}_{\rm STT}$ (see Fig. 1 b) and $\mathbf{m}_{\rm DMI} \perp \mathbf{m}_{\rm STT}$.

The $\mathbf{M}_1$ and $\mathbf{M}_2$ and, consequently, $\mathbf{m}_{\rm DMI}$, which are now exposed to the action of the internal exchange field, start to rotate around $\mathbf{p}$ with the angular velocity

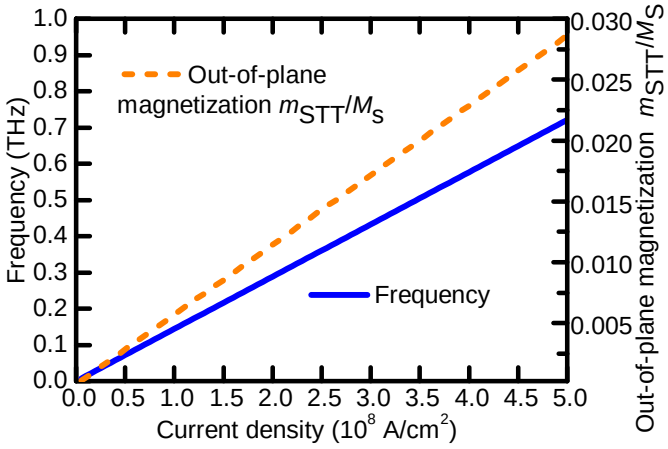

FIG. 2. Calculated frequency of the generated AC signal f (solid line, left axis) and normalized magnitude of the out-of-plane magnetization $m_{\rm STT}/M_{\rm s}$ (dashed line, right axis) in an SHO based on a canted AFM (Hematite) as functions of the DC driving current density $j_{\rm DC}$ in the adjacent Pt layer for the Hematite film thickness of $d_{\rm AFM} = 5$ nm.

$\omega = 2\pi f = \tau/\alpha_{\rm eff}$. This rotation is almost uniform in time, due to the low value of the in-plane anisotropy in Hematite.

The rotation frequency f, as well as the net magnetization $m_{\rm STT}$, are shown as functions of the electric current density flowing in the Pt layer in Fig. 2. To obtain these curves it is necessary to know the value of the spin-mixing conductance $g_{\uparrow\downarrow}$ at the Pt/Hematite interface. Although there exist several studies of the electronic structure of Hematite [34–36], we did not find a reliable value of $g_{\uparrow\downarrow}$ in literature. For numerical simulations we choose a value $g_{\uparrow\downarrow} = 6.9 \cdot 10^{14}{\rm cm}^{-2}$, which was previously obtained for the Pt/NiO interface [37] and is in a good agreement with the rough estimations made by the method developed in [38]. The assumption for the $g_{\uparrow\downarrow}$ magnitude also allows us to make a direct comparison of both the general properties and the intrinsic spin dynamics for the SHO based on Hematite and a similar auto-oscillator based on the NiO [22].

As one can see from Fig. 2, the generation frequency f can be controlled by the density $j_{\rm DC}$ of the electric current injected in the Pt layer. For instance, the current density $j_{\rm DC}$ that is required to get the generation at the frequency of $f = 0.5$ THz is $j_{\rm DC} = 3.5{\cdot}10^8$ A/cm^2, which has been previously achieved in experiment [15].

IV. DIPOLAR ELECTROMAGNETIC RADIATION OF A ROTATING NET MAGNETIZATION IN A CANTED AFM

To investigate the possibility of power extraction from an SHO based on an Pt/AFM layered structure, let us, first, consider the electric current in a Pt layer produced by the ISHE caused by a current-driven rotation of the AFM sublattice magnetizations. The density of the spin current flowing back from the AFM layer to the adjacent Pt layer $\mathbf{j}_{\rm s}^{\rm out}$ can be written as:

$$\mathbf{j}_{\rm s}^{\rm out} = \frac{\hbar g_{\uparrow\downarrow}}{4\pi M_{\rm s}^2} \sum_{i=1,2} \left(\mathbf{M}_i \times \dot{\mathbf{M}}_i \right). \qquad (6)$$

In our case of an easy-plane AFM with DMI, the total net magnetization caused by the DMI is precessing along a cone of the height $m_{\rm STT}$ and cone base radius $m_{\rm DMI}$ (see Fig. 1). Therefore, the AC component of the current $\mathbf{j}_{\rm s}^{\rm out}$ (see Eq. (6)) is proportional to the product of *two small quantities* $\sim m_{\rm DMI} m_{\rm STT}$ and, consequently, in the considered frequency range it is negligibly small (see Fig. 2). In particular, we obtain the maximum output power less than 100 pW at $f = 1$ THz for a square Hematite sample having 200 μm^2 surface area. Such a low value of the output power makes the ISHE practically useless as a method of the signal extraction in the frequency range $2\pi f \ll \gamma\mu_0 H_{\rm ex}$, and it is necessary to find other ways to extract an output AC signal from an SHO based on a canted AFM with negligible in-plane anisotropy.

Fortunately, in a canted AFM crystal, having a small net magnetization, the current-induced precession of this magnetization can be detected not only through the ISHE, but also *directly* through the dipolar radiation produced by this precessing magnetization. The rotating magnetization of the AFM-based SHO $\mathbf{m}_{\rm DMI}$ creates an oscillating dipolar magnetic field that can be received, channeled, and, then, utilized, if the generating SHO is coupled to an appropriate resonator.

The problem of the direct dipolar emission of an AC signal generated by a precessing magnetization has been considered in [39] for the case of a conventional microwave-frequency STNO. It was shown in [39] that the dipolar emission mechanism might become preferable for the case of magnetic devices operating at frequencies above 0.1 THz, which makes this mechanism promising for application in the THz-frequency AFM-based SHOs.

To calculate the AC power $P_{\rm AC}$ that can be emitted by the SHO into a free space, different transmission lines (rectangular waveguide, parallel plate waveguide, dielectric waveguide) and different resonators (rectangular, parallel plate, dielectric) we used a simple model of a direct dipolar emission from a system of two effective magnetic dipoles developed in [39, 40]. In the framework of this approach we used the expressions for the fields of a magnetic dipole obtained in [40, 41] and the standard expressions for the electromagnetic fields of fundamental modes in the considered transmission lines and resonators presented in [41]. Also, to simplify the theoretical analysis of the electromagnetic field excitation in a rectangular dielectric waveguide and resonator by a net AC magnetization $\mathbf{m}_{\rm DMI}$ we used the approximate magnetic wall boundary conditions [41]. Unfortunately, the exact analytical solution for this problem has not been found, so far.

In our approximate calculation we assumed that the rotating net magnetization of the AFM-based SHO $\mathbf{m}_{\rm DMI}$

is spatially uniform (macrospin approximation), and that the sizes of the effective magnetic dipoles (defined by the in-plane dimensions of the SHO) are substantially smaller than the wavelength λ of the AC signal. To evaluate the maximum magnitude of the emitted AC power we took the magnitude of the AC magnetization $\mathbf{m}_{\rm DMI}$ from the numerical solution of Eq. (1).

Using the above described model we performed full electrodynamic calculations of the power emitted by an AFM-based SHO into different microwave/THz-frequency resonators and transmission lines (see Appendix for details), and found that in all cases the maximum emitted AC power can be expressed by the following generalized expression:

$$P_{\rm AC} = P_{\rm m}\frac{V}{V_{\rm eff}}Q\ . \qquad (7)$$

Here $P_{\rm m} = \mu_0 m_{\rm DMI}^2 V f$ is the characteristic AC power generated in the SHO by the rotating magnetization $\mathbf{m}_{\rm DMI}$, f is the frequency of the generated AC signal, $V = \pi r_{\rm SHO}^2 d_{\rm AFM}$ is the volume of the AFM layer, Q is the quality factor of a particular resonance system, and $V_{\rm eff}$ is the frequency-dependent effective volume of a particular resonance system coupled to the AFM-based SHO. Basically the expressions for $V_{\rm eff}$ obtained for the electromagnetic energy emission into free space (far-field zone), nano-loop (near-field zone), rectangular and dielectric waveguides, parallel plate line, rectangular, parallel plate, and dielectric resonators represent the results of electrodynamic calculation, and can be used to compare the efficiency of AFM-based signal generators coupled to different resonance systems (see Table I).

It follows from Eq. (7) that a significant output AC power $P_{\rm AC}$ can be obtained only when the resonator coupled to the AFM-based SHO has a reasonably high quality factor ($Q \gg 1$), and the SHO is operating at a sufficiently high frequency, as $P_{\rm m}$ *increases* with the increase of the generation frequency f. This generation frequency can be controlled by the magnitude of the driving current density (see Fig. 2). It is, also, important to have a sufficiently small "effective volume" $V_{\rm eff}$ of the SHO resonator, which, in the ideal case, should be comparable to the volume V of the AFM layer.

The extracted AC power should be substantially smaller in the case of radiation into a transmission line, where $Q = 1$, and/or the effective volume $V_{\rm eff}$ is, typically, substantially larger than the volume of the AFM layer.

To decrease the effective volume of the resonance system one could fill it with a dielectric having a large dielectric permittivity ε. This approach is well-known in the microwave and terahertz-frequency technology [41]. A simple qualitative analysis shows that a high-Q THz-frequency dielectric resonator could be an effective system for the extraction of the generated AC power from an AFM-based SHO. It is also obvious, that the intrinsic AC power $P_{\rm m} \sim fV$, and the efficiency of the AC power extraction, using the dipolar radiation mechanism, are

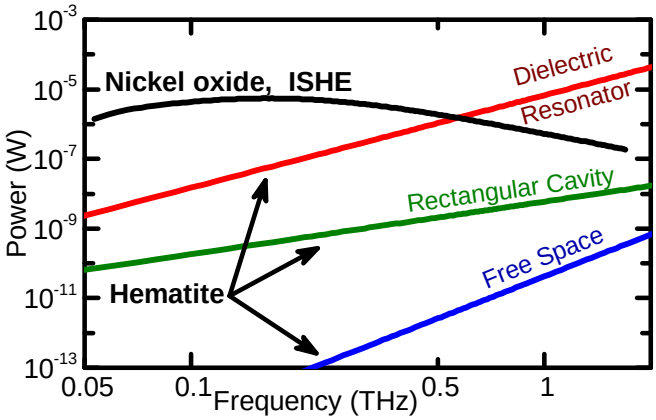

FIG. 3. Generated power vs. frequency for an SHOs based on a layer (thickness $d_{\rm AFM} = 5$ nm) of a canted AFM providing dipolar radiation into different types of resonance systems: dielectric resonator (red line), rectangular cavity (green line), free space (blue line). For comparison, a similar curve is presented for an SHO based on a layer of bi-anisotropic AFM (NiO) where the generated AC signal is extracted through the ISHE in the adjacent Pt layer (black line demonstrating decrease of the generated power with frequency).

higher for the AFM-based SHOs, than for the conventional ferromagnetic STNO. The reasons for that are, first of all, the much higher frequencies f generated by AFM-based SHOs ($f \sim 1$ THz in an SHO, while it is $f \sim 10$ GHz in a typical STNO, see Fig. 2), and a substantially larger active magnetic layer volume V in an AFM-based SHO, compared to an STNO (typical radius of a conventional circular STNO is about 100 nm, while the radius of an antiferromagnetic SHO could be 100 and more times larger).

Despite a relatively small magnitude of the net magnetization $\mathbf{m}_{\rm DMI}$ rotating inside a canted AFM and, consequently, a relatively small magnitude of the intrinsic power $P_{\rm m}$, one could obtain a substantial output power $P_{\rm AC}$ of the total auto-generator based on layer of a canted AFM in the case of a sufficiently high generation frequency f.

Using Eq. (7) we calculated the maximum AC power $P_{\rm AC}$ radiated by a Hematite-based SHO into different resonance structures (free space, rectangular and dielectric resonator) as functions of the generated frequency. These curves are shown in Fig. 3. In Fig. 3 blue line shows the dependence $P_{\rm AC}(f)$ for a Hematite SHO ($d_{\rm AFM} = 5$ nm) radiating into free space, while the green line and red line show the dependence $P_{\rm AC}(f)$ for the Hematite-based SHO coupled to a rectangular cavity and a high-Q dielectric resonator, respectively. For comparison, a similar curve (black line) is presented for an SHO based on a layer of a bi-anisotropic AFM (NiO) ($d_{\rm AFM} = 5$ nm), where the generated AC signal is extracted through the ISHE in the adjacent Pt layer. It is clear, that the signal extraction method based on the ISHE has an advantage at relatively low frequencies, but the method based on

TABLE I. Expressions for $V_{\rm eff}$ and values for the AC power emitted by an SHO at $f = 0.5$ THz calculated using Eq. (7)

Case	Expression for $V_{\rm eff}$	Parameters	Maximum power, W
Free space	$3c^3/8\pi^3 f^3$	$f = 0.5$ THz, $c = 3 \cdot 10^8$m/s, $Q = 1$	$2.6 \cdot 10^{-12}$
Nano-loop	$r_{\rm SHO}^2 R_{\rm L}/2\mu_0\pi^2 f$	$R_{\rm L} = 6030\ \Omega$, $Q = 1$	$1.4 \cdot 10^{-10}$
Rectangular waveguide	$2a^2 b\chi/\pi^2$	$a = 0.47$ mm, $b = 50$ nm, $\chi = \eta/\sqrt{1-\eta^2}$, $\eta = c/2af \approx 0.64$, $Q = 1$	$2.3 \cdot 10^{-8}$
Dielectric waveguide	$2a^2 b\chi_\varepsilon/\pi^2$	$a = 0.47$ mm, $b = 50$ nm, $\chi_\varepsilon = \eta_\varepsilon/\sqrt{1-\eta_\varepsilon^2}$, $\eta_\varepsilon = c/2af\sqrt{\varepsilon} \approx 0.2$, $\varepsilon = 10$, $Q = 1$	$2.9 \cdot 10^{-8}$
Parallel plate line	$8abc/\pi^2 f$	$a = 0.47$ mm, $b = 50$ nm, $Q = 1$	$1.2 \cdot 10^{-9}$
Rectangular resonator	$8a^4 b\chi^3 f^2/c^2$	$a = 0.47$ mm, $b = 50$ nm, $Q = 10$	$2.26 \cdot 10^{-9}$
Parallel plate resonator	$2abc/f$	$a = 0.47$ mm, $b = 50$ nm, $Q = 2$	$9.7 \cdot 10^{-10}$
Dielectric resonator	$2a^2 b\chi_\varepsilon$	$a = 0.47$ mm, $b = 50$ nm, $\varepsilon = 10$, $Q = 750$	$1.1 \cdot 10^{-6}$

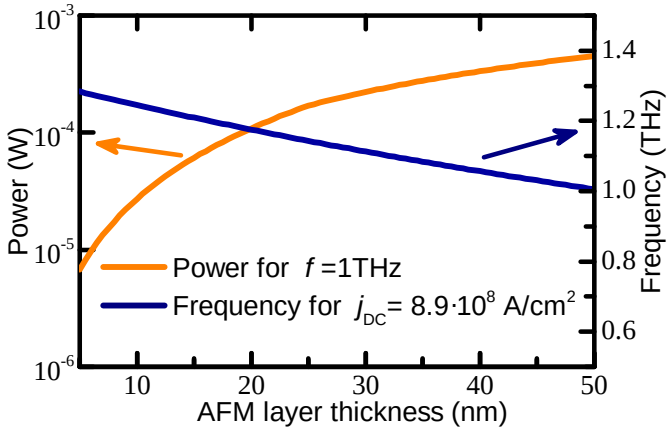

FIG. 4. Power and frequency of a signal generated in an SHO based on a canted AFM (Hematite) as functions of the AFM layer thickness. The power was calculated for the generated frequency $f = 1$ THz, while the frequency was calculated at the driving DC current $j_{\rm DC} = 8.9 \cdot 10^8 {\rm A/cm}^2$.

the dipolar radiation from a canted AFM wins in the limit of high THz frequencies.

There are several approaches to THz-frequency generation, including the use of free electron lasers , quantum cascade lasers [6], superconductor Josephson junctions [8], backward wave oscillators [9], electro-optic rectification of laser radiation [10]

The dependencies of the power and frequency of a signal generated in an SHO based on a canted AFM (Hematite) on the AFM layer thickness are presented in Fig. 4. The power was calculated for the generated frequency $f = 1$ THz, while the frequency was calculated at the driving DC current $j_{\rm DC} = 8.9 \cdot 10^8$ A/cm^2. As it was mentioned above, the generation frequency f depends on the ratio of the spin transfer torque (STT) τ to the effective damping constant $\alpha_{\rm eff}$ as: $2\pi f = \tau/\alpha_{\rm eff}$. The damping constant $\alpha_{\rm eff}$ (see Eq. (4)) includes the contribution of the intrinsic AFM damping α_0, which, we assumed, does not depend on the AFM thickness, and the loss of the spin angular momentum due to the spin pumping – $\alpha_{\rm SP}$. Since the STT and spin pumping share the same origin, and are, practically, the interfacial effects because of the small spin-diffusion length in the AFM insulators, both the STT τ and the spin-pumping-induce damping $\alpha_{\rm SP}$ are inversely proportional to the AFM thickness $d_{\rm AFM}$ (see Eq. (3) and Eq. (4)). Therefore, in the limiting case, when $\alpha_0 = 0$, the generation frequency does not depend on the AFM thickness at all. For most AFM insulators α_0 is relatively small, and for sufficiently thin AFM films the ratio $\alpha_0 \ll \alpha_{\rm SP}$ holds. In this case, as one could see in Fig. 4, the increase of the AFM layer thickness leads to a moderate decrease of the generated frequency, but, at the same time, to a substantial increase of the generated power, which, in turn, is proportional to $d_{\rm AFM}$. Obviously, in the opposite case, when $\alpha_{\rm SP} \ll \alpha_0$, which is realized for a thick AFM layer ($d_{\rm AFM} > 100$ nm for Hematite), the frequency of the oscillations decreases as $1/d_{\rm AFM}$. Interestingly, that the last case is common for the STT oscillators based on the ferromagnetic metals (FM), even having rather thin FM layers, due to the large Gilbert damping constant $\alpha_0 \simeq 0.01$ in the FM metals. It should be also noted, that the calculation results presented in Fig. 4 were obtained in the macrospin approximation, which is quantitatively correct only for sufficiently thin AFM layers (probably thinner than $20 - 30$ nm). However, the relatively weak dependence of the generation frequency and a substantially stronger dependence of the generated power on the thickness of the AFM layer is practically important, and a more accurate micromagnetic calculations should be used in the future to optimize the AFM thickness in the practical AFM-based signal generators.

The general expressions for the effective volume $V_{\rm eff}$ along with the system's parameters and the values of $P_{\rm AC}$ (calculated at a generation frequency of $f = 0.5$ THz) are presented in Table I (see Appendix for details).

The results presented in the Table I and Fig. 3 (blue line) demonstrate that the power emitted from an AFM-based SHO operating at a frequency $f = 0.5$ THz into a free space is very low. If we place an SHO in the center of a gold wire nano-loop of a round shape (radius $r_{\rm L} = 100$ μm, square cross-section of the wire is

TABLE II. Comparison of the proposed THz-frequency AFM-based SHO with existing THz- and GHz-frequency generators

Type of generator	Typical frequency range	Typical AC power	Comments	References
Proposed AFM-based SHO	$0.1-10$ THz	$0.1-500$ μW	$P_{\rm AC}$ increases with frequency f	—
Other AFM-based SHOs	$0.1-1.5$ THz	$0.1-1$ μW	$P_{\rm AC}$ reaches maximum at frequencies $f\sim 0.1$ THz	[21, 22]
Gyrotron	$0.1-0.5$ THz	1 kW – 5 MW	Large complex setup, high voltage, strong DC magnetic field are required	[5]
Backward wave oscillator	$0.03-1.5$ THz	1 mW – 1 W	Sizes $\gtrsim 1$ cm, high voltage is required	[5, 9]
Free electron laser	$1-4$ THz	1 W – 10 kW (peak power)	Large complex setup, high voltage, strong DC magnetic field are required	[4, 5, 10]
Quantum cascade laser	$0.5-3$ THz	$0.1-1$ μW	Complex setup, works at low temperatures ($\lesssim 100$ K)	[6, 7]
Semiconductor-heterostructure laser	4.4 THz	$\gtrapprox 2$ μW	Complex setup, works at low temperatures ($\lesssim 10$ K)	[42]
Electro-optic rectification of laser radiation	$0.1-1$ THz	1 μW – 1 mW	An external THz-frequency pumping source is required	[10]
Uni-travelling-carrier photodiode	$0.1-1$ THz	10 μW – 10 mW	AC power greatly reduces with the increase of frequency f	[10]
Josephson oscillator	$0.1-1$ THz	1 nW – 1 μW	Complex setup, works at cryogenic temperatures	[8]
FM-based SHO	$10^{-3}-10^{-2}$ THz	1 – 10 pW	AC power is too low to date	[11, 15, 25, 26, 43]
FM-based STNO	$10^{-3}-5\cdot 10^{-2}$ THz	100 pW – 1 μW	AC power typically reduces with the increase of frequency f	[11–18]

$S_{\rm L} = 50\times 50$ nm^2, and the characteristic resistance $R_{\rm L} = 2\pi\rho_{\rm Au} r_{\rm L}/S_{\rm L} = 6030$ Ω, where $\rho_{\rm Au} = 24$ $n\Omega\cdot$m is the resistivity of gold) we can increase the emitted power by approximately 10^2 times, because the power can be collected by the loop in a near-field zone (see Table I)[39].

To increase the generated power we can also place an AFM-based SHO in a waveguide (rectangular, parallel plate or dielectric). In this case the electromagnetic field generated by an SHO can excite fundamental propagating modes in these transmission lines, but, as it can be seen from Table I, this approach is not very effective, because for the considered waveguides $Q = 1$, and $V_{\rm eff} \gg V$, which, in accordance to Eq. (7) leads to rather small values of $P_{\rm AC}$.

In order to substantially enhance the emitted power, an SHO should be placed in a microwave/THz-frequency resonator with a sufficiently high Q, which allows one to increase the emitted power Q times (see Eq. (7)). Our calculations performed for rectangular, parallel plate and dielectric resonators having sizes $a\times b\times l$ and reasonably high frequency-dependent quality factors $Q\equiv Q(f)$[44] demonstrated, that power emitted into a rectangular or parallel plate resonators having metal walls is comparable to the power that can be extracted from an SHO placed in transmission line, mainly due to the increase of the ohmic losses in the resonator walls (both resonators) and radiation losses (parallel plate resonator).

The power emitted into a resonator can be increased if the effective volume $V_{\rm eff}$ of the resonator is reduced, while its quality factor remains sufficiently large. To achieve this, it is possible e.g. to place an SHO inside a dielectric resonator having the resonance frequency $f = 0.5$ THz (mode TM$_{101}$), reasonable sizes ($470\,\mu$m $\times$ 50 nm $\times$ 97 μm), and the dielectric permittivity $\varepsilon = 10$ and Q-factor $Q = 750$. In such a case the power emitted by the AFM-based SHO into a dielectric resonator could reach $P_{\rm AC} = 1.1\,\mu$W (see Table I, and a red line in Fig. 3). It is clear from Fig. 3 and Table I, that the design of an AFM-based SHO involving a high-Q dielectric resonator could be promising for the development of practical THz-frequency AC signal sources based on the antiferromagnetic SHOs.

At the same time, at the frequencies higher than 1 THz the use of quasi-optical resonators might turn out to become preferable. Also, as it is clear from Fig. 4, an additional enhancement of the AC power $P_{\rm AC}$ emitted from an AFM-based SHO could be achieved by increasing the thickness $d_{\rm AFM}$ of the AFM layer. This will lead to the increase of the AFM layer volume $V\sim d_{\rm AFM}$ and, therefore, to the increase in the power of magnetization oscillations $P_{\rm m}$ (see Eq. (7)).

Finally, it is interesting, for comparison, to consider a bi-anisotropic AFM crystal with no DMI (e.g. nickel oxide (NiO)) where the AC component of the output spin

current can reach a substantial magnitude, if the AFM sublattice rotation is non-uniform in time [22]. In this case, the AC component of the current $\mathbf{j}_s^{out}$ is proportional to the acceleration in the rotation of the sublattice magnetizations. The SHO based on this effect was proposed in [22], where the small in-plane anisotropy of the NiO makes the sublattice rotation non-uniform in time. The calculated output power of such an NiO SHO is shown on Fig. 3 by a black solid line. To make a direct comparison with the case of an "easy-plane" Hematite SHO we assumed that both types of AFM-based SHOs have the same surface area. As one can see from Fig. 3, the output power of the NiO SHO decreases with the increase of the generation frequency, and this device and this method of the AC signal extraction become non-competitive for generation frequencies above 0.5 THz.

To understand, what is the area of possible practical applications of the proposed THz-frequency generators based on the AFM SHO, it is very useful to compare their characteristics (frequency range, AC power, specific features and experimental requirements) with the characteristics of existing THz-frequency generators and GHz-frequency generators based on the FM materials. The results of this comparison are summarized in Table II. As one can see, in contrast with many considered generator systems, the proposed AFM-based generators integrated with a high-Q dielectric resonators does not require complex setups, can be easily fabricated, and will have sizes less than 1 mm. Although the operation frequency of these generators is limited by the AFM resonance frequency f_{AFMR} and, for typical materials, it is below 1 THz [25], the AC power extracted from such a device could substantially exceed 1 μW, which is a characteristic maximum value of the AC power that could be obtained from an FM-based STNOs at the frequencies $\sim$ 1 GHz. Also, the frequency and power values of the above considered AFM-based SHO greatly exceed the corresponding characteristics of the FM-based SHOs. The above proposed oscillator based on the canted AFM materials has substantial advantages over the other AFM-based SHOs recently investigated in [21, 22]. In contrast to the previously considered AFM-based SHOs [21, 22], where the SHO's output power is reduced at frequencies $f > f_{AFMR}$, our SHO has an important advantage - its output power increases with the increase of the generation frequency f, which makes this generator promising for applications at the high end of the THz frequency range. We believe that the above mentioned interesting and useful properties of the proposed THz-frequency AFM-based generator could be employed in the development of low- and medium-power sources of THz-frequency signals for practical applications in THz spectroscopy, medical imaging, etc.

V. CONCLUSIONS

In conclusion, we have demonstrated theoretically that an SHO based on a canted antiferromagnet (e.g. Hematite) could be used for the development of THz-frequency AC signal sources, where the power of a generated AC signal can be extracted from an SHO through the dipolar oscillating magnetic field created by the current-driven rotating net magnetization of the canted AFM. We have shown that the efficiency of this mechanism of the AC power extraction is increased with the increase of the signal frequency, and depends on the Q-factor and the effective volume of the attached microwave/THz-frequency resonance system. Our analysis has also shown, that the output AC power of such a THz-frequency signal source could exceed 1 μW at the frequency $f \sim 0.5$ THz for the Hematite/Pt SHO coupled to a dielectric resonator with reasonable experimental parameters (sizes $470\,\mu\text{m} \times 50\,\text{nm} \times 97\,\mu\text{m}$, dielectric permittivity $\varepsilon = 10$ and Q-factor $Q = 750$). The above proposed SHO based on a current-driven layered structure of a canted AFM and Pt and incorporating an external dielectric resonator has a practically interesting level of the output power, and its efficiency increases with the increase of the generation frequency, in contrast to the NiO SHO, proposed in [22], which relies on the ISHE mechanism for the extraction of the AC power. The obtained results could become critically important for the development and optimization of practical THz-frequency nano- and micro-scale electromagnetic signal sources.

VI. ACKNOWLEDGEMENTS

This work was supported financially by the Grants Nos. EFMA-1641989 and ECCS-1708982 from the NSF of the USA, the Knut and Alice Wallenberg foundation (KAW), by the Center for NanoFerroic Devices (CNFD) and the Nanoelectronics Research Initiative (NRI), by DARPA, by the Taras Shevchenko National University of Kyiv, Ukraine (Grant No. 16BF052-01), by the National Academy of Sciences of Ukraine via Grant No. 7F and the project # 1/17-N, by the Ministry of Education and Science of the Russian Federation in the framework of Increase Competitiveness Program of NUST MISiS (№K2-2017-005), implemented by a governmental decree dated 16th of March 2013, N 211. The publication also contains results of the studies conducted under the "President's of Ukraine" grant for competitive projects (F74/150–2017) and grant F76/63–2017 of the State Fund for Fundamental Research of Ukraine.

VII. APPENDIX

Generalized expression (7) for the maximum AC power P_{AC} that is emitted by an AFM-based SHO contains the effective frequency-dependent volume V_{eff} of a particular

microwave/THz-frequency system coupled to the SHO. In this Appendix we consider the method of $V_{\rm eff}$ calculation for the systems considered in the article. The method is based on evaluation of output AC power $P_{\rm AC}$, which can be extracted from an SHO coupled to a particular microwave/THz-frequency system, using different techniques that depends on a type of considered system, and then estimation of $V_{\rm eff}$ as

$$V_{\rm eff} = V\frac{P_{\rm m}}{P_{\rm AC}}Q\,, \tag{8}$$

where $P_{\rm m} = f\mu_0 m_{\rm DMI}^2 V$ is the characteristic AC power generated in SHO by the rotating net magnetization $m_{\rm DMI}$, f is the frequency of the generated signal, $V = \pi r_{\rm SHO}^2 d_{\rm AFM}$ is the volume of the AFM layer having radius $r_{\rm SHO}$ and thickness $d_{\rm AFM}$, Q is the Q-factor of the system coupled to the generating SHO, and μ_0 is the vacuum permeability. The final expressions for $V_{\rm eff}$ calculated in the scope of this approach for all considered microwave/THz-frequency systems are presented in Table I.

Free space. The total power radiated in a far-field zone by a system of two almost identical magnetic dipoles can be presented as a double power radiated by one dipole. The components of the field generated by a magnetic dipole in a free space (relative permittivity $\varepsilon = 1$, relative permeability $\mu = 1$) are [41]:

$$\begin{aligned}
E_\phi &= -\frac{{\rm i}\omega\mu_0\mathcal{M}}{4\pi}\,{\rm e}^{-{\rm i}kr}\left(\frac{{\rm i}k}{r}+\frac{1}{r^2}\right)\sin\theta\,{\rm e}^{{\rm i}\omega t}\,,\\
H_r &= \frac{{\rm i}\omega\mu_0\mathcal{M}}{2\pi}\,{\rm e}^{-{\rm i}kr}\left(\frac{1}{Z_0 r^2}+\frac{1}{{\rm i}\omega\mu_0 r^3}\right)\cos\theta\,{\rm e}^{{\rm i}\omega t}\,,\\
H_\theta &= \frac{{\rm i}\omega\mu_0\mathcal{M}}{4\pi}\,{\rm e}^{-{\rm i}kr}\left(\frac{{\rm i}\omega\varepsilon_0}{r}+\frac{1}{Z_0 r^2}+\frac{1}{{\rm i}\omega\mu_0 r^3}\right)\sin\theta\,{\rm e}^{{\rm i}\omega t}\,,
\end{aligned} \tag{9}$$

where $\mathcal{M} = m_{\rm DMI}V$ is the magnetic moment of SHO's AFM layer, $\omega = 2\pi f$, $k = \omega/c$, c is the speed of light, $Z_0 = \sqrt{\mu_0/\varepsilon_0}$ is the vacuum impedance, ε_0 is the vacuum permittivity, and ${\rm i} = \sqrt{-1}$. In the far-field zone, at the distances $r > \lambda$ (here λ is the wavelength of the generated signal), one can keep in (9) only terms $\sim 1/r$ and obtain a simplified form of the generated electromagnetic field:

$$\begin{aligned}
E_\phi &= \frac{\omega^2\mu_0\mathcal{M}}{4\pi c r}\,{\rm e}^{-{\rm i}kr}\sin\theta\,{\rm e}^{{\rm i}\omega t}\,,\\
H_r &= 0\,,\\
H_\theta &= -\frac{\omega^2\mathcal{M}}{4\pi c^2 r}\,{\rm e}^{-{\rm i}kr}\sin\theta\,{\rm e}^{{\rm i}\omega t}\,.
\end{aligned}$$

The energy transfer from the dipoles into the free space is described by the time-averaged value of the Poynting vector $\mathbf{P} = \{P_r, 0, 0\}$ having only one non-zero r-component:

$$P_r = \frac{1}{2}|{\rm Re}\,\{E_\phi H_\theta^*\}\,| = \frac{\omega^4\mu_0\mathcal{M}^2}{32c^3r^2\pi^2}\sin^2\theta\,.$$

The total power emitted by two magnetic dipoles can be written as

$$P_{\rm AC} = 2\oint\limits_S \mathbf{P}d\mathbf{S} = \frac{\omega^4\mu_0\mathcal{M}^2}{6c^3\pi}\,,$$

which using (8) gives in the case $Q = 1$ an expression for the effective volume: $V_{\rm eff} = 3c^3/8\pi^3 f^3$.

Nano-loop. By using nano-loop one can extract the power generated by an AFM-based SHO in the near-field zone. In this case the output signal in nano-loop can be received via AC voltage induced in the loop due to the oscillations of magnetic field (magnetic flux) inside the loop. This AC magnetic field is created by the oscillating magnetic dipoles and can be described by expressions (9), where one should keep only terms $\sim 1/r^3$ and neglect the others that is usual approach for such problems [41]. The AC voltage induced in the nano-loop by one oscillating magnetic dipole can be estimated as

$$|V_{\rm dip}| = 2\pi\mu_0\omega\Big|\int\limits_{r_{\rm SHO}}^{r_{\rm L}} H(r)rdr\Big| \sim \mu_0\pi f\mathcal{M}\Big|\int\limits_{r_{\rm SHO}}^{r_{\rm L}}\frac{dr}{r^2}\Big|\,,$$

where $H(r) \sim m_{\rm DMI}r_{\rm SHO}^2 d_{\rm AFM}/4r^3$ is the component of dipole's magnetic field, which is perpendicular to the loop's cross-section. Taking into account that $r_{\rm SHO} \ll r_{\rm L}$ and assuming that the total AC voltage induced in loop $|V_{\rm L}|$ can be twice larger than $|V_{\rm dip}|$ (both voltages generated by the dipoles are in phase), the voltage $|V_{\rm L}|$ can be written as $|V_{\rm L}| \approx 2\pi^2\mu_0 f m_{\rm DMI}r_{\rm SHO}d_{\rm AFM}$. Then the power of extracted AC signal can be estimated as

$$P_{\rm AC} \approx \frac{|V_{\rm L}|^2}{2R_{\rm L}} = P_{\rm m}V\frac{2\pi^2\mu_0 f}{R_{\rm L}r_{\rm SHO}^2}\,,$$

where $R_{\rm L}$ is the resistance of the nano-loop. It follows from the written equation and (8), where one can let $Q = 1$, that the effective volume $V_{\rm eff}$ is given by an expression: $V_{\rm eff} = R_{\rm L}r_{\rm SHO}^2/2\pi^2\mu_0 f$.

SHO in transmission lines. In order to estimate the power of AC signal generated in the AFM-based SHO and emitted into transmission line it is convenient to introduce the magnetic current density $\mathbf{j}^m = {\rm i}2\pi f m_{\rm DMI}(\mathbf{x}+\mathbf{z})$, which depends on the magnetization of the AFM layer and describes the source of the electromagnetic AC field (here $\mathbf{x}$ and $\mathbf{z}$ are the unit vectors of x- and z-axis, respectively). Then, using the Lorentz' lemma for electromagnetic fields in the transmission line [41], one can obtain the amplitude of excited sth mode in the line:

$$C_s = \frac{\int\limits_V \mathbf{j}^m\mathbf{H}_{-s}dV}{\int\limits_{S_\perp}\{[\mathbf{E}_s\times\mathbf{H}_{-s}]-[\mathbf{E}_{-s}\times\mathbf{H}_s]\}\,\mathbf{z}dS}\,. \tag{10}$$

Here index s corresponds to the wave propagating in the direction $+z$, and index $-s$ corresponds to the wave propagating in the direction $-z$; $S_\perp$ is the cross-section surface of the transmission line. The AC power delivered

from an SHO to the sth mode of a transmission line can be evaluated as:

$$P_{\mathrm{AC},s} = \frac{1}{2}\mathrm{Re}\left\{\int\limits_{S_\perp}[\mathbf{E}_\mathrm{s}\times\mathbf{H}_\mathrm{s}^*]\,\mathbf{z}dS\right\} = \\ = \frac{1}{2}\mathrm{Re}\left\{\int\limits_{S_\perp}\left(E_{\mathrm{sx}}H_{\mathrm{sy}}^* - E_{\mathrm{sy}}H_{\mathrm{sx}}^*\right)dS\right\}, \tag{11}$$

where the field components are proportional to the C_s.

Rectangular waveguide. The field components of TE_{10} mode having a unit amplitude in a hollow rectangular waveguide of cross-section $a\times b$ (a is a its wide wall size, b is its narrow wall size) can be written as [41]:

$$H_{\pm z} = \cos\left(\frac{\pi}{a}x\right)\mathrm{e}^{\mp\mathrm{i}\beta z},$$
$$E_{\pm y} = -\mathrm{i}\omega\mu_0\frac{a}{\pi}\sin\left(\frac{\pi}{a}x\right)\mathrm{e}^{\mp\mathrm{i}\beta z},$$
$$H_{\pm x} = \pm\mathrm{i}\beta\frac{a}{\pi}\sin\left(\frac{\pi}{a}x\right)\mathrm{e}^{\mp\mathrm{i}\beta z},$$

where $\beta = \sqrt{\frac{\omega^2}{c^2} - \frac{\pi^2}{a^2}}$ is a propagation constant. Using these expressions for the field components of TE_{10} mode, one can obtain from (11):

$$P_{\mathrm{AC}} = Z_0\frac{a^3 b}{\lambda^2}C_s^2\sqrt{1-\left(\frac{\lambda}{2a}\right)^2}.$$

By using the field components of TE_{10} mode and calculating C_s from (10), one can obtain the final expression for maximum AC power emitted from a generating SHO in TE_{10} mode of a rectangular metal waveguide:

$$P_{\mathrm{AC}} = \frac{f^2\mu_0\pi^2\mathcal{M}^2}{abc}\sqrt{1-\left(\frac{c}{2af}\right)^2},$$

which also allows one to write the expression for V_{eff} assuming $Q=1$: $V_{\mathrm{eff}} = 2a^2b\chi/\pi^2$, where $\chi = \eta/\sqrt{1-\eta^2}$, $\eta = c/2af$.

Using the same approach, one can obtain expressions for P_{AC} in any other transmission lines.

Dielectric waveguide. The analysis procedure for the TE_{10} mode in a dielectric waveguide, excited by the rotating net magnetization in the AFM layer of an SHO, is identical to the algorithm used for the analysis of wave excitation in a rectangular waveguide. Using magnetic wall boundary condition [41], one can write the field components of TE_{10} mode in the waveguide having cross-section $a\times b$ and made of dielectric with relative permittivity ε:

$$E_{\pm z} = \cos\left(\frac{\pi}{a}x\right)\mathrm{e}^{\mp\mathrm{i}\beta z},$$
$$E_{\pm x} = -\mathrm{i}\beta\frac{a}{\pi}\sin\left(\frac{\pi}{a}x\right)\mathrm{e}^{\mp\mathrm{i}\beta z},$$
$$H_{\pm y} = \mp\mathrm{i}\omega\varepsilon_0\varepsilon\frac{a}{\pi}\sin\left(\frac{\pi}{a}x\right)\mathrm{e}^{\mp\mathrm{i}\beta z}.$$

Substituting these expressions in (10), (11), one can obtain the final expression for P_{AC}:

$$P_{\mathrm{AC}} = \frac{\mu_0 f^2\pi^2\mathcal{M}^2}{abc}\sqrt{1-\left(\frac{c}{2af\sqrt{\varepsilon}}\right)^2},$$

and write the expression for V_{eff} assuming $Q=1$: $V_{\mathrm{eff}} = 2a^2b\chi_\varepsilon/\pi^2$, where $\chi_\varepsilon = \eta_\varepsilon/\sqrt{1-\eta_\varepsilon^2}$, $\eta_\varepsilon = c/2af\sqrt{\varepsilon}$.

Parallel plate line. The parallel plate transmission line consists of two parallel metallic plates of width a with a dielectric layer of permittivity $\varepsilon\approx 1$ located between the plates (its thickness is b). We analyze the excitation of a fundamental T-wave in the line only and assume that there is no electromagnetic field out of the line's cross-section. Using (10) the amplitude of excited T-wave can be obtained in the form:

$$|C_s| = \frac{\pi f\mu_0}{2ab}\mathcal{M}.$$

The power transmitted into a parallel plate line is given by (11):

$$P_{\mathrm{AC}} = |C_s|^2\frac{ab}{2Z_0} = \frac{\pi^2\mu_0\mathcal{M}^2 f^2}{8abZ_0},$$

which also allows one to write the expression for V_{eff} assuming $Q=1$: $V_{\mathrm{eff}} = 8abc/\pi^2 f$.

SHO in resonators. When an AFM-based SHO is coupled to the resonator system one can use Maxwell's equations for the electromagnetic field components $\mathbf{E}$, $\mathbf{H}$, excited by a magnetic current density $\mathbf{j}^m$ [41]:

$$\mathrm{rot}\,\mathbf{E} + \mathrm{i}\omega\mu_0\mu\mathbf{H} = -\mathbf{j}^m,\ \mathrm{rot}\,\mathbf{H} - \mathrm{i}\omega\varepsilon_0\varepsilon\mathbf{E} = 0. \tag{12}$$

The field components can be presented as a series expansion by eigen fields of the resonator [45]:

$$\mathbf{E} = \sum_n A_n\mathbf{E}_n,\ \mathbf{H} = \sum_n B_n\mathbf{H}_n, \tag{13}$$

where for simplicity we neglect the terms dependent on gradient functions ($\mathrm{grad}\,\Psi_{e,h}$). The eigen fields $\mathbf{E}_n$ and $\mathbf{H}_n$ are the solutions of the uniform equations

$$\mathrm{rot}\,\mathbf{E}_n + \mathrm{i}\omega_n\mu_0\mu\mathbf{H}_n = 0,\ \mathrm{rot}\,\mathbf{H}_n - \mathrm{i}\omega_n\varepsilon_0\varepsilon\mathbf{E}_n = 0. \tag{14}$$

They satisfy the following orthogonality conditions [45]: [45]:

$$\int\limits_V \mathbf{E}_n^*\varepsilon_0\varepsilon\mathbf{E}_{n'}dV = N_n^e\Delta_{nn'},\ \int\limits_V \mathbf{H}_n^*\mu_0\mu\mathbf{H}_{n'}dV = N_n^h\Delta_{nn'},$$
$$\Delta_{nn'} = \begin{cases}1, & n=n'\\ 0, & n\neq n'\end{cases}. \tag{15}$$

By substituting (13) in (12), then multiplying $\mathbf{H}_n^*$ by the first obtained equation and $\mathbf{E}_n^*$ by the second one, and after that integrating newly obtained equations over

the resonator volume V_r and taking into account (15), one can get:

$$\begin{aligned}\sum_n A_n \int\limits_V \mathbf{H}_n^* \mathrm{rot}\,\mathbf{E}_n dV + \mathrm{i}\omega B_n N_n^h = -\int\limits_V \mathbf{H}_n^* \mu_0 \mu \mathbf{j}^m dV\,,\\ \sum_n B_n \int\limits_V \mathbf{E}_n^* \mathrm{rot}\,\mathbf{H}_n dV - \mathrm{i}\omega A_n N_n^e = 0\,.\end{aligned} \tag{16}$$

Using (14) one can write (16) in the form:

$$\begin{aligned}-\mathrm{i}\omega_n A_n N_n^h + \mathrm{i}\omega B_n N_n^h = -\mathrm{i}\omega G_n\,,\\ \mathrm{i}\omega_n B_n N_n^e - \mathrm{i}\omega A_n N_n^e = 0\,,\end{aligned}$$

where $G_n = \int\limits_V \mathbf{H}_n^* \mu_0 \mu \mathbf{m}_\mathrm{DMI}\, dV$. This system of equation has a solution:

$$A_n = \frac{\omega\omega_n}{\omega_n^2 - \omega^2}\frac{G_n}{N_n^h}\,,\ B_n = \frac{\omega^2}{\omega_n^2 - \omega^2}\frac{G_n}{N_n^h}\,. \tag{17}$$

To analyse the resonator excitation at the frequency $\omega \approx \omega_n$ one can introduce the Q-factor of the resonator $Q_n = \omega_n/|\omega_n - \omega|$ and assume that $Q_n \gg 1$. In this case (17) transforms to $A_n \approx B_n \approx Q_n G_n / 2N_n^h$.

The AC power pumped in the nth resonance mode by the SHO can be calculated as:

$$P_{\mathrm{AC},n} = \frac{1}{2}(A_n^2 N_n^e + B_n^2 N_n^h). \tag{18}$$

Rectangular resonator. Field components of TE_{101} mode of a hollow rectangular resonator having volume $a \times b \times l$ can be written in the form [41]:

$$\begin{aligned}E_y &= A_n \sin\left(\frac{\pi}{a}x\right)\sin\left(\frac{\pi}{l}z\right)\,,\\ H_x &= -\mathrm{i}\frac{A_n}{Z_0}\frac{\lambda}{2l}\sin\left(\frac{\pi}{a}x\right)\cos\left(\frac{\pi}{l}z\right)\,,\\ H_z &= \mathrm{i}\frac{A_n}{Z_0}\frac{\lambda}{2a}\cos\left(\frac{\pi}{a}x\right)\sin\left(\frac{\pi}{l}z\right)\,.\end{aligned}$$

The AC power pumped in the resonator by SHO can be calculated using the maximum value of the electric field:

$$P_\mathrm{AC} = \frac{f}{Q}\frac{\varepsilon_0}{2}\int\limits_0^a dx \int\limits_0^b dy \int\limits_0^l dz |E_{\mathrm{y\ max}}|^2 = \frac{\varepsilon_0 f A_n^2}{8Q} abl\,,$$

where $l = \lambda a/\sqrt{4a^2 - \lambda^2}$.

Assuming that SHO can be considered as a "point" object with magnetic moment $\mathcal{M}$, located in the point (x_0, y_0, z_0) inside the cavity, one can do the following estimations:

$$\begin{aligned}G_n &= \mathrm{i}\mu_0 m_\mathrm{DMI}\frac{1}{Z_0}\frac{\lambda}{2}\times\\ &\times\left(\frac{1}{l}\sin\left(\frac{\pi}{a}x_0\right)\cos\left(\frac{\pi}{l}z_0\right) - \frac{1}{a}\cos\left(\frac{\pi}{a}x_0\right)\sin\left(\frac{\pi}{l}z_0\right)\right)\,,\\ N_n^h &= \mu_0 abl\lambda^2\left(1/l^2 + 1/a^2\right)/16Z_0^2\,,\\ A_n &\approx \frac{4Qm_\mathrm{DMI}Z_0 al}{b\lambda(a^2+l^2)}\times\\ &\times\left[\frac{1}{l}\sin\left(\frac{\pi}{a}x_0\right)\cos\left(\frac{\pi}{l}z_0\right) - \frac{1}{a}\cos\left(\frac{\pi}{a}x_0\right)\sin\left(\frac{\pi}{l}z_0\right)\right]\,.\end{aligned}$$

In the typical case, when $x_0 = a/2$, $z_0 = 0$ (SHO is attached to the center–bottom of the resonator's front wall), we can obtain:

$$P_\mathrm{AC} = 2\frac{\varepsilon_0 Q f M^2 Z_0^2 a^2}{b^2\lambda^2(a^2+l^2)^2} abl\,,$$

which also gives $V_\mathrm{eff} = 8a^4 b\chi^3 f^2/c^2$.

Parallel plate resonator. Here we analyze the excitation of T_{001} mode in a parallel plate resonator of cross-section $a \times b$ and length $l = \lambda/2$. The electromagnetic field of the T-mode has the form:

$$E_y = A_n \sin\left(\frac{\pi}{l}z\right)\,,\ H_x = -\frac{A_n}{Z_0}\cos\left(\frac{\pi}{l}z\right)\,.$$

Microwave power P_AC pumped into the resonator's mode from an AFM-based SHO can be calculated using the maximum value of the electric field:

$$P_\mathrm{AC} = \frac{\varepsilon_0 f}{2Q}\int\limits_0^a dx \int\limits_0^b dy \int\limits_0^l dz |E_{\mathrm{y\ max}}|^2 = \frac{\varepsilon_0 f A_n^2}{4Q} abl\,,$$

where $A_n \approx \dfrac{Q\mathcal{M}Z_0}{abl}\cos\left(\dfrac{\pi}{l}z_0\right)$. In the typical case, when $z_0 = 0$ (SHO is attached to the front side of the resonator), one can obtain:

$$P_\mathrm{AC} = \frac{\varepsilon_0 f Q \mathcal{M}^2 Z_0^2}{4abl}\,.$$

Then it follows that $V_\mathrm{eff} = 2abc/f$.

Dielectric resonator. We assume that the dielectric resonator has sizes $a \times b \times l$, where $l = a\lambda/\sqrt{4a^2\varepsilon - \lambda^2}$ and is made of dielectric with permittivity ε. Using the same approach as for rectangular resonator and magnetic wall boundary conditions [41], one can write field components of the TM_{101} mode:

$$\begin{aligned}E_x &= \frac{\mathrm{i}A_n}{\omega\varepsilon\varepsilon_0}\sin\left(\frac{\pi}{a}x\right)\sin\left(\frac{\pi}{l}z\right)\,,\\ E_z &= -\frac{\mathrm{i}A_n}{\omega\varepsilon\varepsilon_0}\cos\left(\frac{\pi}{a}x\right)\sin\left(\frac{\pi}{l}z\right)\,,\\ H_y &= A_n \sin\left(\frac{\pi}{a}x\right)\sin\left(\frac{\pi}{l}z\right)\,.\end{aligned}$$

Then the AC power pumped in the resonator from the SHO can be evaluated as:

$$P_{\rm AC} = \frac{f}{Q}\frac{\mu_0}{2}\int\limits_0^a dx \int\limits_0^b dy \int\limits_0^l dz |H_{\rm y\ max}|^2 = \frac{\mu_0 f A_n^2}{8Q} abl\,.$$

Assuming that SHO can be considered as a "point" object with magnetic moment $\mathcal{M}$, located in the point (x_0, y_0, z_0), we obtain: $A_n \approx \frac{2Q\mathcal{M}}{abl}\sin\left(\frac{\pi}{a}x_0\right)\sin\left(\frac{\pi}{l}z_0\right)$. In the typical case, when $x_0 = a/2$, $z_0 = 0$ (SHO is attached to the center–bottom of the resonator's front wall), an expression for the output power transforms to its final form:

$$P_{\rm AC} = \frac{\mu_0 f Q \mathcal{M}^2}{2abl}\,.$$

Thus, $V_{\rm eff} = 2a^2 b\chi_\varepsilon$, where $\chi_\varepsilon = \eta_\varepsilon/\sqrt{1-\eta_\varepsilon^2}$, $\eta_\varepsilon = c/2af\sqrt{\varepsilon}$.

[1] C. Sirtori, Applied physics: Bridge for the terahertz gap, Nature **417**, 132 (2002).

[2] R. Kleiner, Filling the Terahertz Gap, Science **318**, 1254 (2007).

[3] Yu. V. Gulyaev, P. E. Zilberman, G. M. Mikhailov, and S. G. Chigarev, Generation of terahertz waves by a current in magnetic junctions, JETP Lett. **98**, 742 (2014).

[4] E. A. Nanni, W. R. Huang, K.-H. Hong, K. Ravi, A. Fallahi, G. Moriena, R. J. D. Miller, and F. X. Kärtner, Terahertz-driven linear electron acceleration, Nat. Comms. **6**, 8486 (2015).

[5] M. V. Kartikeyan, E. Borie, and M. Thumm, *Gyrotrons. High Power Microwave and Millimeter Wave Technology.* (Springer, 2004).

[6] H.-W. Hübers, Terahertz technology: Towards THz integrated photonics, Nat. Photon. **4**, 503 (2010).

[7] L. Consolino, S. Jung, A. Campa, M. De Regis, S. Pal, J. H. Kim, K. Fujita, A. Ito, M. Hitaka, S. Bartalini, P. De Natale, M. A. Belkin, M. S. Vitiello, Spectral purity and tunability of terahertz quantum cascade laser sources based on intracavity difference-frequency generation, Sci. Adv. **3**, e1603317 (2017).

[8] L. Ozyuzer, A. E. Koshelev, C. Kurter, N. Gopalsami, Q. Li, M. Tachiki, K. Kadowaki, T. Yamamoto, H. Minami, H. Yamaguchi, T. Tachiki, K. E. Gray, W.-K. Kwok, and U. Welp, Emission of Coherent THz Radiation from Superconductors, Science **318**, 1291 (2007).

[9] B. Gorshunov, A. Volkov, I. Spektor, A. Prokhorov, A. Mukhin, M. Dressel, S. Uchida, A. Loidl, Terahertz BWO-Spectrosopy, Int. J. Infrared Milli. Waves **26**, 1217 (2005).

[10] M. Tonouchi, Cutting-edge terahertz technology, Nat. Photon. **1**, 97 (2007).

[11] T. Chen, R. K. Dumas, A. Eklund, P. K. Muduli, A. Houshang, A. A. Awad, P. Dürrenfeld, B. G. Malm, A. Rusu, J. Åkerman, Spin-Torque and Spin-Hall Nano-Oscillators, Proc. IEEE **104**, 1919 (2016).

[12] M. Tsoi, A. G. M. Jansen, J. Bass, W.-C. Chiang, V. Tsoi, and P. Wyder, Generation and detection of phase-coherent current-driven magnons in magnetic multilayers, Nature **406**, 46 (2000).

[13] S. I. Kiselev, J. C. Sankey, I. N. Krivorotov, N. C. Emley, R. J. Schoelkopf, R. A. Buhrman, and D. C. Ralph, Microwave oscillations of a nanomagnet driven by a spin-polarized current, Nature **425**, 380 (2003).

[14] W. H. Rippard, M. R. Pufall, S. Kaka, S. E. Russek, and T. J. Silva, Direct-Current Induced Dynamics in $Co_{90}Fe_{10}/Ni_{80}Fe_{20}$ Point Contacts, Phys. Rev. Lett. **92**, 027201 (2004).

[15] V. E. Demidov, S. Urazhdin, H. Ulrichs, V. Tiberkevich, A. Slavin, D. Baither, G. Schmitz, and S. O. Demokritov, Magnetic nano-oscillator driven by pure spin-current, Nat. Mater. **11**, 1028 (2012).

[16] S. M. Mohseni, S. R. Sani, J. Persson, T. N. Anh Nguyen, S. Chung, Ye. Pogoryelov, P. K. Muduli, E. Iacocca, A. Eklund, R. K. Dumas, S. Bonetti, A. Deac, M. A. Hoefer, and J.Åkerman, Spin Torque-Generated Magnetic Droplet Solitons, Science **339**, 1295 (2013).

[17] J. D. Costa, S. Serrano-Guisan, B. Lacoste, A. S. Jenkins, T. Böhnert, M. Tarequzzaman, J. Borme, F. L. Deepak, E. Paz, J. Ventura, R. Ferreira, and P. P. Freitas, High power and low critical current density spin transfer torque nano-oscillators using MgO barriers with intermediate thickness, Sci. Rep. **7**, 7237 (2017).

[18] S. Bonetti, P. Muduli, F. Mancoff, and Johan Åkerman, Spin torque oscillator frequency versus magnetic field angle: The prospect of operation beyond 65 GHz, Appl. Phys. Lett. **94**, 102507 (2009).

[19] H. V. Gomonay and V. M. Loktev, Spin transfer and current-induced switching in antiferromagnets, Phys. Rev. B **81**, 144427 (2010).

[20] E. V. Gomonay and V. M. Loktev, Spintronics of antiferromagnetic systems, Low Temp. Phys. **40**, 17 (2014).

[21] R. Cheng, D. Xiao, and A. Brataas, Terahertz Antiferromagnetic Spin Hall Nano-Oscillator, Phys. Rev. Let. **116**, 207603 (2016).

[22] R. Khymyn, I. Lisenkov, V. Tiberkevich, B. A. Ivanov, and A. Slavin, Antiferromagnetic THz-frequency Josephson-like Oscillator Driven by Spin Current, Sci. Rep. **7**, 43705 (2017).

[23] P. Wadley, B. Howells, J. Železný, C. Andrews, V. Hills, R. P. Campion, V. Novák, K. Olejník, F. Maccherozzi, S. S. Dhesi, S. Y. Martin, T. Wagner, J. Wunderlich, F. Freimuth, Y. Mokrousov, J. Kuneš, J. S. Chauhan, M. J. Grzybowski, A. W. Rushforth, K. W. Edmonds, B. L. Gallagher, and T. Jungwirth, Electrical switching of an antiferromagnet, Science **351**, 587 (2016).

[24] D. Kriegner, K. Výborný, K. Olejník, H. Reichlová, V. Novák, X. Marti, J. Gazquez, V. Saidl, P. Němec, V. V. Volobuev, G. Springholz, V. Holý, and T. Jungwirth, Multiple-stable anisotropic magnetoresistance memory in antiferromagnetic MnTe, Nat. Comms. **7**, 11623 (2016).

[25] T. Jungwirth, J. Wunderlich, and K. Olejník, Spin Hall

effect devices, Nat. Mater. **11**, 382 (2012).
[26] V. E. Demidov, S. Urazhdin, A. Zholud, A. V. Sadovnikov, and S. O. Demokritov, Nanoconstriction-based spin-Hall nano-oscillator, Appl. Phys. Lett. **105**, 172410 (2014).
[27] L. Berger, Emission of spin waves by a magnetic multilayer traversed by a current, Phys. Rev. B **54**, 9353 (1996).
[28] J. C. Slonczewski, Current-driven excitation of magnetic multilayers, J. Magn. Magn. Mater. **159**, L1 (1996).
[29] H. Nakayama, K. Ando, K. Harii, T. Yoshino, R. Takahashi, Y. Kajiwara, K. Uchida, Y. Fujikawa, and E. Saitoh, Geometry dependence on inverse spin Hall effect induced by spin pumping in $Ni_{81}Fe_{19}$/Pt films, Phys. Rev. B **85**, 144408 (2012).
[30] P. W. Anderson, F. R. Merrit, J. P. Remeika, and W. A. Yager, Magnetic Resonance in αFe_2O_3, Phys. Rev. **93** 717, (1954).
[31] A. H. Morrish, *Canted Antiferromagnetism: Hematite* (World Scientific, 1995).
[32] E. A. Turov, A. V. Kolchanov, M. I. Kurkin, I. F. Mirsaev, and V. V. Nikolaev, *Symmetry and physical properties of antiferromagnets*, (Cambridge International Science Publishing, Ltd, 2010).
[33] H. Kumagai, H. Abe, K. Ôno, I. Hayashi, J. Shimada, and K. Iwanaga, Frequency Dependence of Magnetic Resonance in α-Fe_2O_3, Phys. Rev. **99**, 1116, (1955).
[34] G. Rollmann, A. Rohrbach, P. Entel, and J. Hafner, First-principles calculation of the structure and magnetic phases of hematite, Phys. Rev. B, **69**, 165107 (2004).
[35] M. N. Huda, A. Walsh, Y. Yan, S.-H. Wei, and M. M. Al-Jassim, Electronic, structural, and magnetic effects of 3*d* transition metals in hematite, J. Appl. Phys. **107**, 123712 (2010).
[36] M. Catti, G. Valerio, and R. Dovesi, Theoretical study of electronic, magnetic, and structural properties of α-Fe_2O_3 (hematite), Phys. Rev. B **51**, 7441 (1995).
[37] R. Cheng, J. Xiao, Q. Niu, and A. Brataas, Spin Pumping and Spin-Transfer Torques in Antiferromagnets, Phys. Rev. Lett. **113**, 057601 (2014).
[38] J. Xiao, G. E. W. Bauer, K. Uchida, E. Saitoh, and S. Maekawa, Theory of magnon-driven spin Seebeck effect, Phys. Rev. B **81**, 214418 (2010).
[39] O. Prokopenko, E. Bankowski, T. Meitzler, V. Tiberkevich, and A. Slavin, Spin-Torque Nano-Oscillator as a Microwave Signal Source, IEEE Magn. Lett. **2**, 3000104 (2011).
[40] N. Amin, H. Xi and M. X. Tang, Analysis of Electromagnetic Fields Generated by a Spin-Torque Oscillator, IEEE Trans. on Magn. **45**, 4183 (2009).
[41] S. Ramo, J. R. Whinnery, and T. Van Duzer, *Fields and Waves in Communication Electronics* (John Wiley & Sons, 1984).
[42] R. Köhler, A. Tredicucci, F. Beltram, H. E. Beere, E. H. Linfield, A. G. Davies, D. A. Ritchie, R. C. Iotti, and F. Rossi, Terahertz semiconductor-heterostructure laser, Nature **417**, 156 (2002).
[43] R. H. Liu, W. L. Lim, and S. Urazhdin, Spectral Characteristics of the Microwave Emission by the Spin Hall Nano-Oscillator, Phys. Rev. Lett. **110**, 147601 (2013).
[44] We choose the qualitative approximation for the frequency dependent Q-factor as $Q(f) = Q_0 \cdot (f_0/f)^{3/2}$ for the rectangular ($Q_0 = 10^5$ at $f_0 = 1$ GHz), $Q(f) = Q_0 \cdot (f_0/f)$ for the parallel plate ($Q_0 = 10^3$ at $f_0 = 1$ GHz) resonators, and $Q(f) = Q_0 \cdot (f_0/f)^{1/3}$ for the dielectric resonator ($Q_0 = 6 \cdot 10^3$ at $f_0 = 1$ GHz).
[45] A. G. Gurevich and G. A. Melkov, *Magnetization Oscillations* and Waves (CRC Press, 1996).